Available online at www.eccomasproceedia.org
Eccomas Proceedia EUROGEN (2023) 206-222

ECCOMAS
Proceedia

EUROGEN 2023
15th ECCOMAS Thematic Conference on
Evolutionary and Deterministic Methods for Design, Optimization and Control
N. Gauger, K. Giannakoglou, M. Papadrakakis, J. Periaux (eds.)
Chania, Crete Greece, 1–3 June 2023

HYDRODYNAMIC OPTIMIZATION OF ACTIVELY DEFORMING FLAPPING-FOIL THRUSTERS FOR AUV PROPULSION

Dimitra Anevlavi*, Evangelos Filippas, and Kostas Belibassakis

School of Naval Architecture and Marine Engineering, NTUA, Zografos 15772, Greece

*Corresponding author: Dimitra Anevlavi. e-mail: danevlavi@mail.ntua.gr

Abstract

Bio-inspired thrusters based on flapping-foils have been proposed as an alternative to conventional rotary propellers for autonomous underwater vehicles (AUVs). By mimicking the swimming mode found among a group of vertebrates, such as sharks and marine mammals, flapping-foils have the potential to achieve very high propulsive efficiency, thus allowing for an extension of the overall operational capabilities of AUVs that come with energy range limitations. At the same time, their low frequency operation provides stealth in terms of acoustic noise which is essential for oceanic exploration and observation of marine life. This work is dedicated to the hydrodynamic optimization of a concept flapping-foil thruster under nonlinear constraints regarding the thrust coefficient and effective angle of attack. We investigate the effects of a wide range of geometric and kinematic parameters including prescribed active deformation, in the sense bending and twisting to the overall performance of the wing. Each candidate design is evaluated using a cost-effective GPU-accelerated boundary element solver (BEM) that is developed to facilitate the optimization process.

Keywords: Active deformation, flapping-foils, biomimetic thruster, hydrodynamic optimization, boundary element method (BEM), GPU-accelerated solver.

Peer-review under responsibility of the organizing committee of EUROGEN 2023.
doi: 10.7712/140123.10200.18952

1 INTRODUCTION

Bio-inspired thrusters based on flapping-foils have been proposed for the propulsion of autonomous underwater vehicles (AUVs) due to certain advantages they hold over conventional rotary propellers. To name a few, they have the potential to achieve high efficiency, advanced maneuverability, and their eco-friendly low-frequency operation emitting low acoustic noise translates into adequate stealth for oceanic exploration and observation of marine life; (Won-Shik, et al. 2012), (Neira, et al. 2021). The thrust-producing *thunninform* kinematics found among a group of vertebrates, such as sharks and marine mammals; see, e.g., (Sfakiotakis, Lane and Davies 1999) and (Lauder 2000), have been successfully modeled as a combination of heaving and pitching rigid body motions with an extensive database of numerical and experimental research that has inspired many swimming robot prototypes, such as the MIT RoboTuna (Barrett 1996). The geometry of caudal and pectoral fins also provides abundant inspiration for the design of new efficient wings with favorable lift/drag ratios, good dynamic stall characteristics. For instance, the distinctive morphology of the humpback whale pectoral fins allow them to delay dynamic stall by introducing vortex generation in the vicinity of the leading edge (Wei, New and Cui 2015), (Shi, et al. 2016). Humpback-whale inspired fins have made their debut in the twin-rudder of the Club Swan 36 yacht from Nautor Swan (see: https://www.nautorswan.com/yachts/models/clubswan36/).

However, fins in nature are elastic and can deform both actively and passively under hydrodynamic load excitation, contributing to the exceptional abilities of aquatic swimmers, both in terms of cruising at high efficiency and advanced maneuverability (Shyy, et al. 2014). Applications of actively deforming (or shape changing in the sense of morphing) wings in the field of naval architecture are quite limited. They can be found among technologies of wing stabilizers with actively controlled flaps, such as the type-S retractable fin stabilizer by (SKF n.d.), and the anti-rolling MR-Series of (Mitsubishi n.d.). In addition, interesting designs have emerged from the studies conducted for the America's Cup racing sailboats, where safety factors are kept to minimum to attain maximum performance (Parolini and Quarteroni 2005). Many racing and fast-cruising foiling sailboats use state-of-the-art actively controlled foils and appendages; see, e.g., the methodology proposed by (Amoroso, et al. 2021) for the seakeeping of a flying yacht or the split-flap concept for the T-foil of a sailing yacht (Prabahar, Persson and Larsson 2022).

However futuristic the concept of actively deforming wings seems, research on this topic contributes to the vision of bio-inspired and more energy efficient thrusters and energy-saving devices for the maritime industry. To provide a short background on the use of active deformation for the control of lifting surfaces, it is important to mention that technologically, this concept was initially introduced in aeronautics as a means of meeting the varying demands of flight scenarios; e.g., (Moran 1984), (Barbarino, et al. 2011) and (Li, et al. 2018).

The demands of aviation are different from marine propulsion; however, the abundant literature on morphing airfoils and wings provides valuable insight for the present project, which aims to reveal trends for hydrofoil energy-minimizing kinematics. In addition, deforming morphing foils have a wide range of applicability ranging from small-scale wave/current energy harvesting systems to full-scale energy-saving systems for ships in wavy seas; (Ntouras, Papadakis and Belibassakis 2022), (Belibassakis, Filippas and Papadakis 2021). The following link contains additional information regarding the Seatech Horizon 2020 project entitled "Next generation short-sea ship dual-fuel engine and propulsion retrofit technologies" (https://seatech2020.eu/) that studies flapping-foils as auxiliary ship thrusters with wave energy harvesting capabilities.

In the present work, we attempt to integrate some of these features into the design of a flapping-foil thruster for a realistic AUV propulsion scenario. Our contribution consists of developing a cost-effective potential-based solver with GPU-acceleration features to predict the hydrodynamic forces and the propulsive performance of wings that undergo prescribed but arbitrary motions. The GPU-BEM computational tool is then used for the hydrodynamic optimization; in terms of propulsive efficiency maximization, of the flapping-foil thruster with geometric and kinematic parameters as design variables under constraints determined based on the examined propulsion scenario. The design variables examined are the sweep angle and the taper ratio that determine the wing planform, the amplitudes of the heaving and pitching motions, forcing frequency (Strouhal number) as well as the amplitudes of chordwise/spanwise bending and twisting (active deformation). The constraints target the thrust coefficient requirement and the maximum allowable effective angle of attack. The findings of the optimization studies are presented and discussed with an aim to reveal trends for the design of efficient flapping-foil thrusters. The findings of this work highlight certain trends that have the potential to enhance the propulsive performance of flapping-foil thrusters, whereas the study of active deformation effects broadens the design space of wings for future thruster applications.

2 FLAPPING-FOIL THRUSTER

Aiming towards a complete redesign of the main propulsion system of an autonomous underwater vehicle (AUVs) that satisfies the initial design specifications; based on a realistic propulsion scenario, we came up with the design concept shown in Figure 1. The total resistance consists of friction resistance (based on the ITTC curve) and wave resistance predicted using the methodology presented in (Belibassakis, Gerostathis, et al. 2013). We assume that for the AUV mission a cruising speed of U=2.52m/s is to be maintained with C_T=0.32 thrust coefficient at the highest propulsive efficiency possible. The details of the examined propulsion scenario are shown in Table 1. The reference thruster that serves as the basis for the optimization study that follows, corresponds to a rigid wing design that performs prescribed heaving/pitching motions and satisfies the thrust requirement.

The examined cruising speed is low and therefore the device is in no risk of cavitation. However, if higher speeds were to be examined cavitation prevention criteria should be taken into account in future work; see, e.g., (Liao, Martins and Young 2021). In this work we use NACA 0012 sections, and the planform shape is parametrized using the sweep angle and the taper ratio (Moran 1984). However, we are aware of the fact that NACA series hydrofoil sections yield high pressures at the suction side near the vicinity of the leading edge which at high inflow speeds is at risk of cavitation. In that sense, for high cruising flapping-foils near the free-surface more suitable sections will be examined in future work.

Table 1. Propulsion scenario

AUV Characteristics	
Geometry	prolate spheroid (5:1:1)
Length overall	$L_{OA} = 5m$
Wetted surface	$S_{wet} = 12.55m^2$
Submergence depth	$d / L = 0.16$
Operation velocity	$U = 2.52m / s$
Froude number	$Fr(L) = 0.36$
Friction coefficient $\left(C_F = R_F / 0.5\rho U^2 S_{wet}\right)$	$C_F = 0.003$

Wave resistance	$C_W = 0.0058$
Total resistance $(C_{TOT} = C_F + C_W)$	$C_{TOT} = 0.0083$
Thrust requirement	$C_{Treq} = 0.32$

Reference flapping-foil thruster

Dimensions (chord, span)	$c = 0.33m,\ s = 1.0m$
Heaving amplitude	$h_0 / c = 0.75$
Pitching amplitude	$\theta_0 = 23^o$
Phase difference	$\psi = -90\,\text{deg}$
Strouhal number $(Str = 2h_0 f / U)$	$Str = 0.26$
Pivot axis	$c / 3$

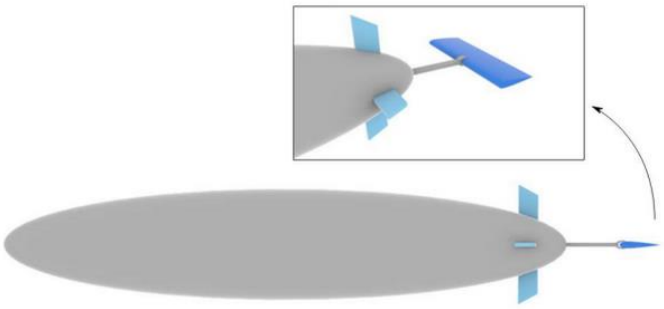

Figure 1. Schematic representation of the AUV body and thruster configuration (highlighted with blue).

2.1 Fish-inspired kinematics

The heave and pitch motions are based respectively on the following harmonic functions

$$h(t) = h_o \sin(\omega t) \tag{1}$$

$$\theta(t) = \theta_o \sin(\omega t + \psi) \tag{2}$$

where the pivot axis for the pitch is positioned at $X_R = c/3$. A forward translation motion $s(t) = -Ut$; towards the negative *y*-axis, simulates the AUV propulsion scenario, thus the free-stream velocity is assumed to be zero and shear current effects are neglected. The following transformation maps the wing surface in the body-fixed coordinate system *xyz* to the global coordinate system *XYZ*,

$$\{X^i\} = [Q^i] \cdot \{x^i\} + \{\Delta^i\}, \tag{3}$$

$$[Q^i] = \begin{bmatrix} \cos\theta(t) & 0 & -\sin\theta(t) \\ 0 & 1 & 0 \\ \sin\theta(t) & 0 & \cos\theta(t) \end{bmatrix}, \{\Delta^i\} = f_s(t) \cdot \begin{bmatrix} s(t) \\ 0 \\ h(t) \end{bmatrix}, \tag{4}$$

where $f_s(t) = 1 - \exp(-f_o(t/T)^2), f_o = 1.5$ is filter function permitting smooth transition between rest and a fully developed state of oscillatory motions.

2.2 Active deformation

The body-fixed coordinate system *xyz* is such that the center (0,0,0) is placed at the intersection of the pivot axis and the root section of the wing; as shown schematically in Figure 2. The positive x-axis is directed towards the chord length of the wing's sections facing the trailing edge and the y-axis towards the spanwise direction. The positive z-axis is determined using a clockwise notation.

2.2.1 Spanwise bending/twisting

Regarding the out-of-plane active deformation the linear bending (G_1) and quadratic twisting (F_1) angles from (Stanford and Beran 2010) are considered,

$$G_1 = 2|y_o|/s \tag{5}$$

$$F_1 = \left(2|y_o|/s\right)^2 \tag{6}$$

where $y_o \in [-s/2, s/2]$ with s denoting the span of the wing in the body-fixed reference frame. Each expression is then multiplied with a time-varying harmonic amplitude,

$$\beta(\mathbf{x}_o,t) = \beta_1(t)\cdot G_1(\mathbf{x}_o), \qquad \beta_1(t) = A_{b_1}\sin(\omega_{b_1}\cdot t + \psi_{b_1}) \tag{7}$$

$$\gamma(\mathbf{x}_o,t) = \gamma_1(t)\cdot F_1(\mathbf{x}_o), \qquad \gamma_1(t) = \mathrm{A}_{\gamma_1}\sin(\omega_{\gamma_1}\cdot t + \psi_{\gamma_1}) \tag{8}$$

where A_{b_1}, A_{γ_1} denote the amplitudes and $\psi_{b_1}, \psi_{\gamma_1}$ the phase differences. The frequency is kept the same as the heaving/pitching motions. It is important to note that although these quantities are considered known prior to each simulation, proper tuning is accomplished via optimization. Regarding the deformed mesh (i) the bending angle $\boldsymbol{\beta}(\mathbf{x}_o,t)$ for each cross-section in the yz-plane is translated into a lateral displacement along the span of the wing and (ii) the twisting angle $\boldsymbol{\gamma}(\mathbf{x}_o,t)$ is used to rotate each cross-section in the xy-plane; as shown see Figure 2.

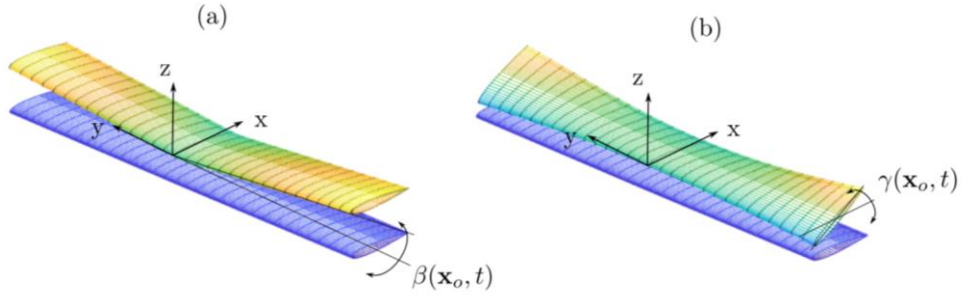

Figure 2. Prescribed active morphing shapes based on (a) linear bending angle and (b) quadratic twisting angle on the body-fixed coordinates system xyz.

2.2.2 Hydrofoil section adjustment

We introduce the following scenario of a time-varying chord-line deformation that is uniform in the spanwise direction shown schematically in Figure 3,

$$y_c(x_o,t) = \begin{cases} 0, & x_o \in (0, X_R] \\ (x_o - X_R)^2 A_c \sin(\omega t + \psi_c), & x_o \in (X_R, c] \end{cases} \tag{9}$$

where $A_c \sin(\omega t + \psi_c)$ denotes the amplitude of morphing, ψ_c the phase difference. In addition, the motion of the fore part of the hydrofoil from the leading edge (LE) to the pivot point is restricted and the morphing affects the rest of the hydrofoil section. Maximum displacement occurs at the trailing edge (TE) region.

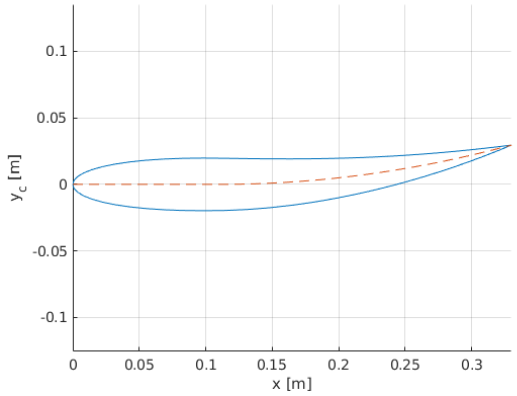

Figure 3. Hydrofoil section at maximum chordwise displacement for Ac=0.08c, ψc=π/2 at t=0s based on Eq. (9) described above.

2.3 Propulsive performance metrics

The instantaneous lift, thrust and moment (with respect to the pivot axis) can be calculated using the following formulas,

$$C_L = L(t) / \left(0.5\rho U^2 cs\right) = -\frac{1}{A}\int_{\partial D_B} C_p \mathbf{n}\cdot\hat{\mathbf{y}} ds, \tag{10}$$

$$C_T = T(t) / \left(0.5\rho U^2 cs\right) = \frac{1}{A}\int_{\partial D_B} C_p \mathbf{n}\cdot\hat{\mathbf{x}} ds, \tag{11}$$

$$C_M = M(t) / \left(0.5\rho U^2 c^2 s\right) = -\frac{1}{Ac}\int_{\partial D_B} C_p \mathbf{n}\cdot\mathbf{r} ds, \tag{12}$$

where A denotes the planform area, and $\boldsymbol{r}$ is the reference vector for the calculation of the moment.

To estimate the propulsive efficiency (Froude efficiency) η for the actively deforming wing, it is essential to take into consideration not only the power required to sustain the rigid-body motions but also an estimate for the power required to produce the changes in geometry. Thus, we calculated the efficiency (η) as follows,

$$\eta = \bar{C}_{Pout} / \bar{C}_{Pin}. \tag{13}$$

where $\bar{C}_{Pout} = P_{out} / \left(0.5\rho U^3 A\right)$, $\bar{C}_{Pin} = P_{in} / \left(0.5\rho U^3 A\right)$ and

$$P_{out} = \frac{1}{T_p U}\int_0^{T_p} T(t) U dt \tag{14}$$

$$P_{in} = \frac{1}{T_p U}\int_0^{T_p} L(t)\dot{h}(t) + M(t)\dot{\theta}(t) + P_{deform}(t) dt \tag{15}$$

with T_p denoting the period of the harmonic motion, *T(t)* is the instantaneous thrust and U the forward motion velocity. All motions share the same frequency. The power required to sustain

the active morphing; see, e.g., (Li, Pan and Zhang 2011) and (Neef and Hummel 2002) for a similar formulation, can be estimated as,

$$P_{deform}(t) = \frac{1}{A} \int_{\partial D_B} C_p(\mathbf{x};t)\ \mathbf{n}(\mathbf{x};t) \cdot \mathbf{V}_{deform}(\mathbf{x};t) ds \tag{16}$$

where $C_p(\mathbf{x};t)$ is the instantaneous pressure coefficient and $\mathbf{V}_{deform}(\mathbf{x};t)$ denotes the instantaneous velocity component solely due to the active deformation; which is directly linked to the active deformation parameters introduced in Section 2.

3 MATERIALS AND METHODS

For the evaluation of the propulsive performance of flapping-foil thrusters that undergo prescribed chordwise and spanwise active deformation, we extended the boundary element method (BEM) developed by (E. Filippas 2019) with results concerning the method validation and various applications in (Filippas, Papadakis and Belibassakis 2020) and (Papadakis, Filippas, et al. 2019). The code includes GP-GPU acceleration features targeting the computationally demanding numerical integration for the calculation of the induced coefficients using the processors of an NVIDIA graphics card and the CUDA API, which significantly reduces the computational time of the simulation. The present solver that has been used in a previous work by the authors (Anevlavi, Filippas and Belibassakis 2023),

- enables numerical calculation of the wing body velocities using backward finite differences with GPU parallelization.
- re-generates the surface mesh at each time-instance to simulate a deforming wing
- re-calculates of the induced coefficients (DtN) matrix at each time-step
- calculates the propulsive performance metrics targeting flapping-foil thrusters

The proposed version of the GPU-BEM is cost-effective and is capable of predicting with acceptable accuracy the propulsive performance of actively deforming flapping-foil thrusters, thus allowing for detailed sensitivity analysis and optimization, which often require many cost function evaluations. The GPU-BEM computational tool performs unsteady simulations for wings with linearized wake or free wake modelling. A similar investigation based on Navier-Stokes models would require costly simulations. The benefits of using potential-based solvers for the problem of energy-minimizing kinematics of animal flight are also addressed in (Stanford and Beran 2010) and (M. Ghommem 2012), where a vortex-lattice method is used to evaluate the performance of candidate thrusters with active morphing and to optimize their kinematics.

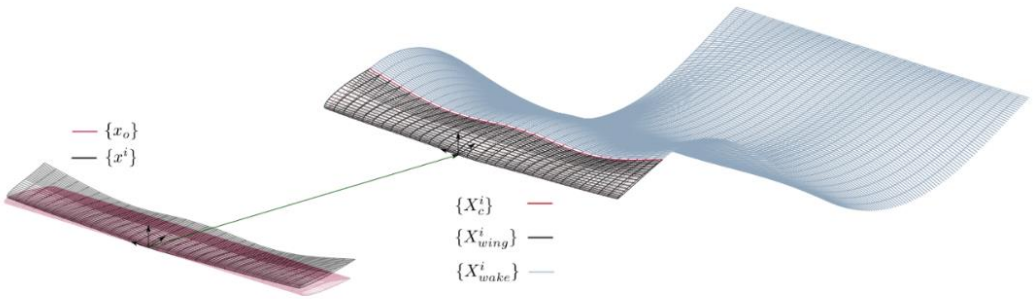

Figure 3. Body-fixed and inertial geometry definitions for the actively morphing wing.

In the present implementation the total velocity is calculated numerically using the consequent configurations of the wing, then

$$\mathbf{V}_{deform}(\mathbf{x};t) = \mathbf{V}_{total}(\mathbf{x};t) - \mathbf{V}_{rigid}(\mathbf{x};t) \tag{17}$$

3.1 GPU-BEM Validation

All computations were performed on an AMD Ryzen 9 3900XT workstation equipped with an NVDIA GeForce RTX 3080. Leading edge separation and tip vortex rollup modelling is not included in the present formulation. The propulsive performance metrics correspond to the average values during the last flapping cycle based on a three-period simulation.

3.1.1 Flow past a flapping (i.e. bending) cambered wing

In the work by (Vest and Katz 1996) were a potential-based computational tool is developed for the analysis of bird flight is it mentioned that time-dependent experimental data for actively deforming wing are very scarce; which still holds today. They compared their unsteady BEM solver with one of the few experiments on actively deforming wings by (Fejtek and Nehera 1980), where a highly cambered NACA 8313 foil was tested. The experiments are motivated from large bird flight at high speeds. The wing had a rectangular planform with a blunt wing tip, 76mm chord length and 305mm span, shaped from a solid balsa plank and covered with a shrink-tight plastic film. We numerically simulated the whole wing as (Vest and Katz 1996) with AR=8, whereas in the experiments only the half-span was tested.

In Figure 5, we compared our method with results from (Fejtek and Nehera 1980) regarding the time histories of the lift and thrust coefficients for a flapping wing in the sense of linear bending with 45^o amplitude at a frequency of 3.3 Hz and inflow velocity U=21.4m/s at zero angle incidence. In Figure 5, numerical data from (Vest and Katz 1996) are also included for a reduced frequency $k=\omega\, c/(2U)$=0.03082, where c denotes the chord length and U the inflow velocity. The numerical results obtained from our method are generally in good agreement with the potential code from (Vest and Katz 1996) and the experimental data. There is some discrepancy between the inviscid numerical results and the experiment, especially during the downstroke which is attributed to viscous phenomena.

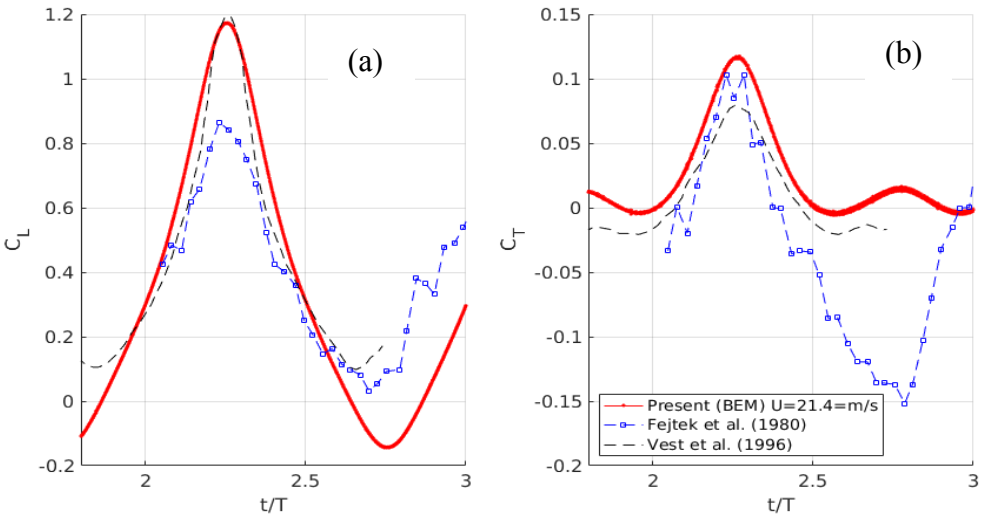

Figure 4. Variations of the (a) lift and (b) thrust coefficients for a flapping (i.e. bending) wing. Comparison with numerical data from (Vest and Katz 1996) and experimental data from (Fejtek and Nehera 1980).

3.1.2 Flow past a flapping (i.e. bending)/twisting rectangular wing

Next, we selected from (Neef and Hummel 2002) a study case inspired from bird flight, at U = 15m/s cruising speed, with reduced frequency of $k = 2\pi fc/(2U) = 0.1$ and $f = 3s-1$. The plunging-type motion is modelled as the first bending mode with flapping amplitude of 15°, whereas the twist motion varies linearly from root to tip. Particularly, the plunging and twisting motions using in the aforementioned study case are based on the linear expression G_1 as follows,

$$\beta(\mathbf{x}_0,t) = f_s A_{b_1} \sin(2\pi ft) G_1(\mathbf{x}_0) \tag{18}$$
$$\gamma(\mathbf{x}_0,t) = f_s[a_o + a_{1,tip} \sin(2\pi ft + \pi/2)] G_1(\mathbf{x}_0)$$

The negative value of the twist angle amplitude corresponds to a nose-up twist at the tip. Also, the mean angle of attack examined were $\alpha_0 = 0^o$ (no lift, thrust only) and $\alpha_0 = -4^o$ (lift and thrust). Regarding the spatial and temporal discretization $dt = 0.125T/100$, $NEA = 49$ (number of panels in the spanwise direction) and $NEC = 60$ (number of panels in the chordwise direction); i.e. approximately 1.25 hours per simulation. In the simulations, wake roll-up is included however; and the trailing vortex sheet is shed from the trailing edge.

For the first comparison shown in Figure 6, $A_{b1} = 0.5s\ tan(15^o)$ and $\alpha_{1,tip} = -4^o$. Numerical results from the vortex lattice solver from (M. Ghommem 2012) that neglects the wing's thickness are also included for comparison purposes. The thrust is over predicted by the BEM solver despite the dense spatial/temporal discretization, which can be attributed, as discussed in (Stanford and Beran 2010), to an under prediction in the strength of the tip vortex swirling (i.e. an under prediction in the strength of the induced drag).This effect is relatively strong in the flow field results provided. Since both models are inviscid, this comparison shows that the present BEM method is capable of reproducing trends in terms of thrust coefficient and Froude efficiency with acceptable accuracy within its range of validity.

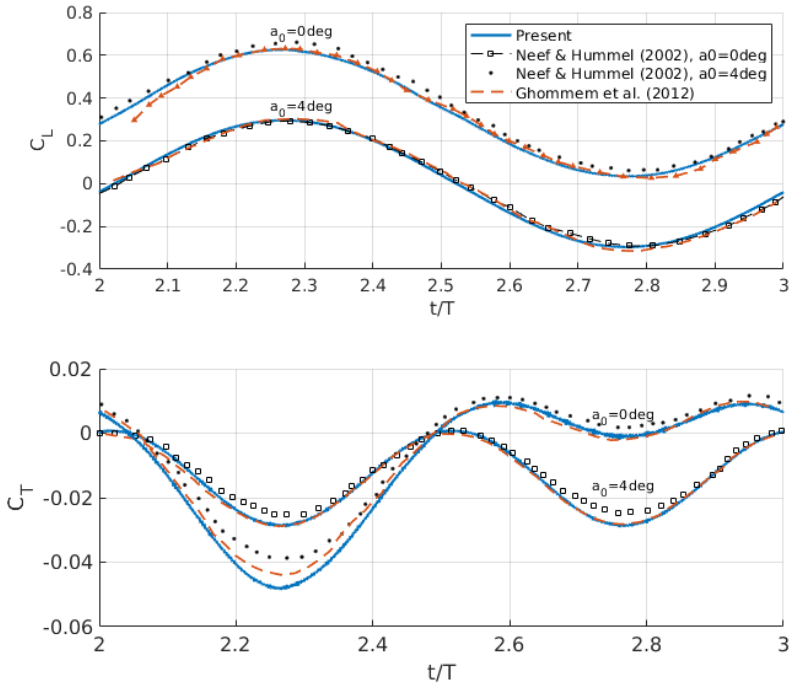

Figure 5. Plunging/twisting wing comparison with (Neef and Hummel 2002) and (M. Ghommem 2012).

3.1.3 Friction drag correction

Consideration of friction drag effects can be included using the following empirical formula that comprises of a skin friction resistance coefficient and a coefficient dependent on the effective angle of attack from (Filippas and K.A. Belibassakis 2014),

$$C_r = C_f\left(\mathrm{Re}\right) + C_a(\mathrm{Re})a^2, \quad C_f\left(\mathrm{Re}\right) = \frac{0.0858}{[\log_{10}\mathrm{Re} - 1.22]^2} \tag{20}$$

This friction coefficient increases at higher angles of attack leading to better predictions. In (Anevlavi, Filippas and Belibassakis 2023) the comparison between the GPU-BEM and the experimental data from (Heathcote, Wang and Gursul 2008) can be found. Other coefficients targeting effects such as leading edge separation can also be formulated in future work to bring inviscid result closer to the reality, assuming that adequate data from either CFD or experiments are provided. The corrections are implemented during the post-processing phase on the instantaneous thrust coefficient $C_{Tvisc}(t) = C_r(t) + C_T(t)$ and then on the efficiency after averaging for the last period of the simulation, i.e. $\eta = \overline{C}_{Tvisc} / \overline{C}_{Pwtot}$.

4 DESIGN OPTIMIZATION APPLICATIONS

The hydrodynamic optimization of actively deforming wings is based on optimally tuning certain key geometric and kinematic parameters. The problem formulation is targeted toward the maximization of propulsive efficiency under thrust and effective angle of attack requirements that are included as constraints.

Particularly,

$$\begin{aligned} &\max\ \eta \\ &\textit{subject to}\quad (1-p)C_{Treq} \le C_T \le (1+p)C_{Treq} \\ &\qquad\qquad a_{eff}(root) \le a_{\max} \\ &b_n \in DS \end{aligned} \tag{21}$$

where b_n is design variable vector and $DS = \{b_n \in R^n \mid lb \le b_n \le ub\}$ the design space defined as an n-dimensional bounding box and. The geometric and kinematic parameters included in the present study are shown in Table 2. The phase difference for the twisting motion is determined via the optimization. Both constraints are enforced upon the average values during the last flapping-cycle of the numerical simulation.

In the applications that follow we assume thet designs with thrust requirement within p = 5% tolerance are acceptable; whereas for the root section the maximum admissible effective angle of attack lie below 12deg. Friction drag corrections given by Eq. (20) are included in the results concerning both the thrust and the efficiency; however, the thrust constraint enforced corresponds to the equivalent inviscid result. The Reynolds number for this study is estimated as Re=861,600 and the coefficients for the friction drag viscous corrections are taken as *Cf=0.0039* and *Ca*=0.13.

The solution of the optimization problem is based on the gradient-based nonlinear programming "*fmincon*" solver offered from (MATLAB n.d.). Particularly, we implemented the sequential quadratic programming algorithm through the "*sqp*" option, which is suitable for handling nonlinear constraints, whereas the gradient computations for the Hessian matrix where based on forward differences. A typical three flapping-cycle simulation with linearized wake (including DtN re-calculation) takes 8min (NEA=31, NEC=60, TSR=0.36 (ω=7.17 rad/s, dt=0.0032s, T3=0.8730s).

4.1 Optimal thruster with active chordwise/spanwise bending

For the first optimization study (case-1) we introduce $b_n = \{A_{sweep}, c_t / c_r, h_0, \theta_0, Str, A_c, A_b\}$ with emphasis on the effects of a superposition of chordwise and spanwise bending on the propulsive performance of the thruster. The phase differences that contribute to efficiency enhancement for this setup have been determined in previous work by the authors (Anevlavi, Filippas and Belibassakis 2023), as ψ_c=180deg and ψ_b=0deg respectively. The frequency of motions is kept the same. The optimal thruster is shown in Table 2 and the corresponding propulsive performance metrics in Table 3. In Figure 7, we provide schematically consecutive instances of the wing's shape during one period of motion. The optimal wing is swept back with taper ratio c_t / c_r=0.335, it operates at the maximum heaving amplitude, a higher pitching amplitude and frequency. Regarding the active deformation, the solution yields the maximum chordwise bending amplitude and Ab=8.9deg. The optimization study required 10 hours on an AMD Ryzen 9 3900XT workstation equipped with an NVDIA GeForce RTX 3080.

Both constraints have been satisfied with a 21% gain in propulsive performance. Essentially, active chordwise deformation resembling the behavior of passively deforming hydrofoils under hydrodynamic load excitation; see e.g. (D. E. Anevlavi, et al. 2020), leads to a significant increase in the propulsive performance as the hydrofoil section follows the flapping-foil trajectory of the motion at a thrust reduction penalty. In addition, since active chordline deformation does not alter drastically the effective angle of attack its contribution to the overall propulsive performance is predicted with good accuracy via potential-based solvers. On the other hand, as shown in (Neef and Hummel 2002) and (Heathcote, Wang and Gursul 2008) spanwise bending contributes significantly to the thrust production and affects significantly the maximum effective angle of attack. Particularly, from the GPU-BEM we predict that the maximum effective angle of attack at the tip of the wing is 22deg. High effective angles of attack are responsible for the high propulsive efficiency reported as shown in Table 4. However, large effective angles of attack are related to dynamic stall phenomena which can be predicted only via viscous computations. In any case, the margin of propulsive performance enhancement is high and thus the proposed optimal thruster design has the potential to outperform the reference design in further numerical examination.

4.2 Optimal thruster with active chordwise bending/twisting

The next optimization study (case-2) is concerned with investigating the effects of a combination of active chordwise bending and twisting; for which we introduce the following design variable vector $b_n = \{A_{sweep}, c_t / c_r, h_0, \theta_0, Str, A_c, A_t, \psi_t\}$. Investigations regarding the effects twist have been addressed in recent works such as (Thielicke and Stamhuis 2018), where it is found via experimental computations using that adapting twist is essential to meet the demands of varying mission requirements by keeping the effective angle of attack sufficiently low to avoid reduction of forces due to viscous phenomena. Motivated by this, we performed the present optimization to reveal whether a combination of active chordwise bending and spanwise twisting variation can increase the efficiency at a reduced effective angle of attack at the root and tip; while at the same time satisfy the thrust requirement.

The findings are presented in Table 3 along with the reference design and the thruster from case-1 for comparison purposes. Figure 8 contains instances of the optimal thruster during the last flapping-cycle. We can observe that the solution fails to satisfy the constrain regarding the effective angle of attack at the root, however at the tip the effective angle of attack is lower than the thruster obtained from case-1; indicating that a combination of both bending and twisting

motions has the potential to produce an optimal thruster with maximum effective angle of attack along the span that is sufficiently low. This is left for future work.

The optimal phase difference for the twist motion is found to be 90deg; thus in phase with the pitching motion with an amplitude of 7deg. The rigid-body motion parameters are close to the results of case-1. The efficiency enhancement is 20% and the discussion from the previous section regarding the effective angle of attack that should be examined with caution is remains valid.

4.3 Comparative analysis

Finally, we present in Figure 9 the time-histories of lift, thrust and moment coefficients for the reference design and the optimal thrusters (case-1, case-2). The new thruster designs produce slightly lower average thrust and lift coefficients, as expected. The moment coefficient is calculated with respect to an axis parallel to the y-axis and positioned at *c/3* at the root section. The large deviations from the time-history of C_M of reference design are attributed to the active deformation of the wing and the changes in planform. The average values of the moment coefficient are lower compared to the reference design as shown in Table 3. The instantaneous power coefficients defined in Sec. 2.3 are also provided for completeness.

Table 2. Design variables and constraints for the optimization studies. The quantities in brackets are defined prior to the optimization and remain fixed for all solutions.

Geometric	**Units (SI)**	**Lower bound**	**Reference**	**Optimal Case-1**	**Optimal Case-2**	**Upper bound**
Sweep angle A_{sweep}	deg	0	0	**14.30**	**27.50**	30.00
Taper ratio c_t / c_r	-	0.100	1.000	**0.335**	**0.950**	1.000
Flapping						
h_0	m	0.250	0.750	**0.930**	**1.000**	1.000
θ_0	deg	5.000	23.00	**33.10**	**28.00**	40.00
Str	-	0.234	0.260	**0.279**	**0.270**	0.286
Active deformation						
Ac	m	0	0	**0.085c**	**0.100c**	0.100c
Ab	deg	0	0	**8.900**	-	10.00
At	deg	-10.00	0	-	**7.000**	10.00
ψt	deg	0	0	-	**90.00**	180.0
ψc	deg	-	0	(180.0)	(180.0)	-
ψb	deg	-	0	(0)	-	-

Table 3. Propulsive performance of thruster designs.

id	**Inviscid**			**Viscous Corrected**		**Root**	**Tip**		
	$\overline{C}_T$	η	$\overline{C}_{Pout}$	$\overline{C}_T$	η	aeff (deg)	aeff (deg)	Sarea (m2)	Diff (%)
0	0.329	0.721	0.4558	0.302	0.663	16.23	16.23	0.3300	
1	0.312	0.878	0.3538	0.296	0.834	11.98	22.04	0.2759	+21.77
2	0.314	0.867	0.3615	0.292	0.8087	13.24	19.30	0.3259	+20.24

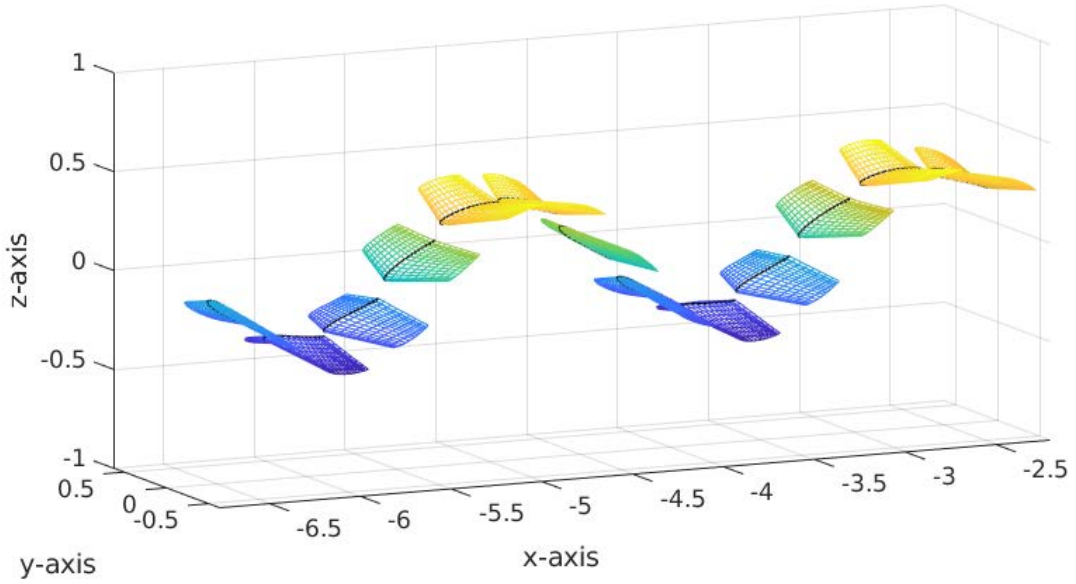

Figure 6. Case-1: Deformed shape instances for a wing with active chordwise and spanwise bending deformation during two flapping-cycles.

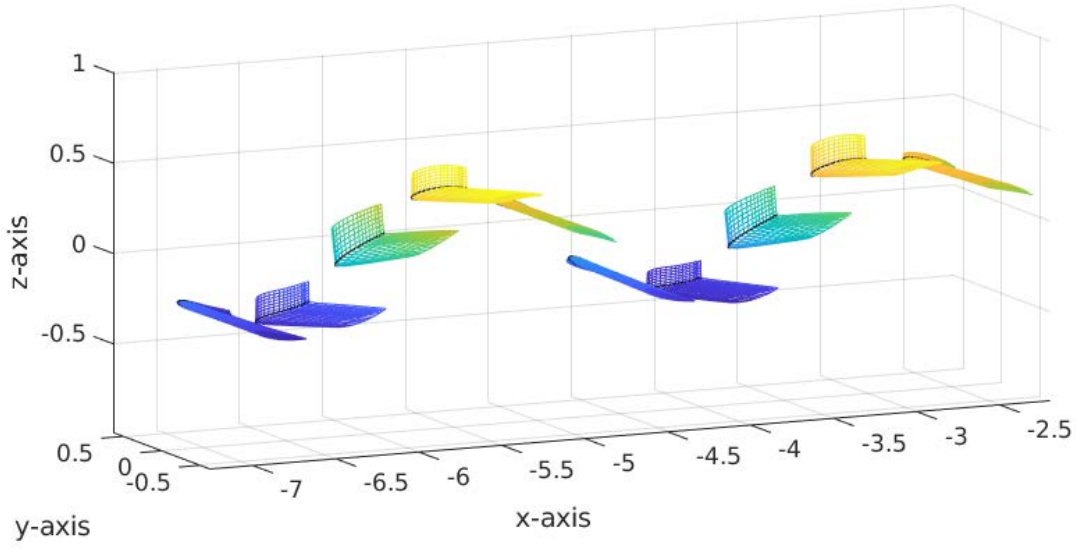

Figure 7. Case-2 Deformed shape instances for a wing with chordwise bending and spanwise twisting deformation during two flapping-cycles.

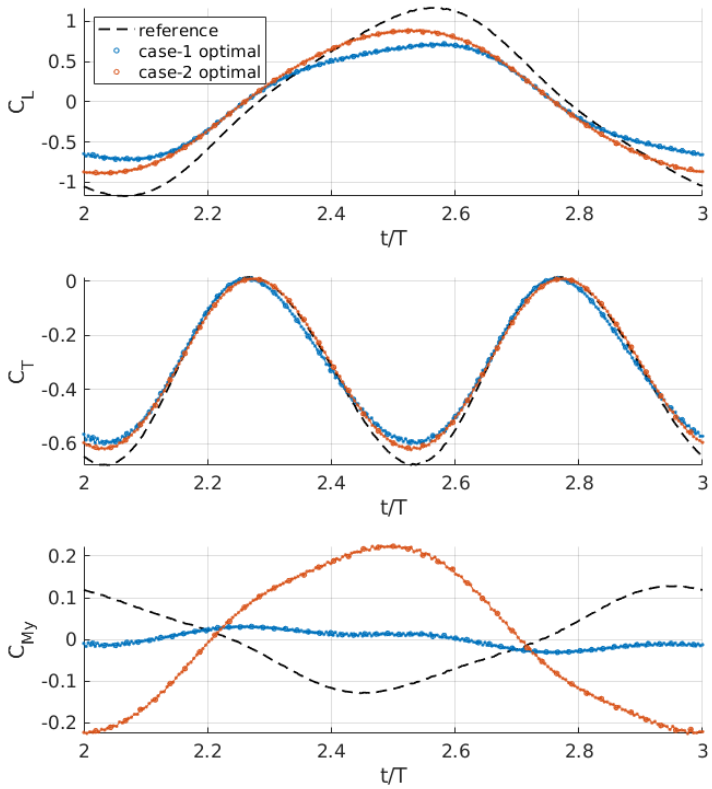

Figure 8. Time-histories of lift, thrust and moment coefficients for the reference design and the optimal thrusters.

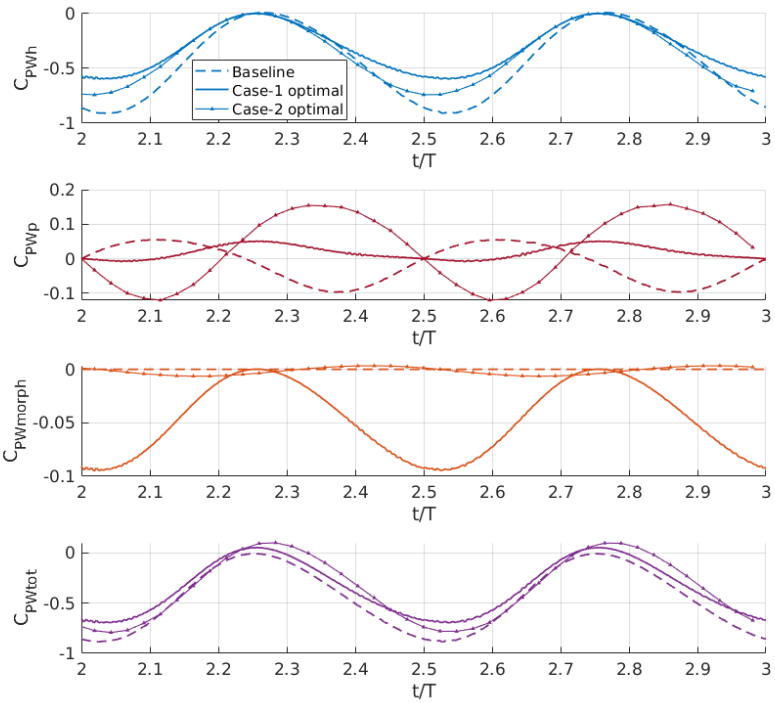

Figure 9. Instantaneous power coefficients for the reference and optimal thrusters during the last flapping-cycle of the simulation.

5. CONCLUSIONS

In the present work, we examined the effects of geometric and kinematic parameters in the sense of heaving/pitching motions as well as parameters of active time-varying bending and twisting deformation on the propulsive performance of flapping-foil thrusters for AUV propulsion using a realistic scenario. The two optimization studies are conducted to reveal whether an optimal tuning of the examined parameters exists, with a focus on propulsive efficiency maximization under a thrust and effective angle of attack constraints. Each candidate design is evaluated using a new cost-effective GPU-accelerated BEM solver suitable for predicted hydrodynamic forces and the propulsive performance of wing performing prescribed but arbitrary motions (flapping, chordwise/spanwise bending, twisting etc.). Friction drag corrections have used in the post-processing phase for the average thrust coefficient and efficiency.

Based on the findings of this work, an optimally tuned combination of active deformation in the sense of bending and twisting for an optimized planform (sweep angle, taper ratio) yields up to 20% performance enhancement, although the instantaneous angles of attack become quite increased and it needs further investigation. The optimal thrusters operating at a higher Strouhal number and a heaving/pitching amplitude compared to the reference design, to compensate for the reduction in thrust due to the increase of propulsive efficiency. Regarding the phase difference, for the optimal design spanwise bending is in phase with the heaving motion, whereas chordwise bending has a phase difference of 180degrees compared to the heaving motion. The optimal phase difference for the twisting motion is found to be 90deg; thus in phase with the pitching motion. The results indicate that flapping-foil thrusters have the potential to operate as highly energy-efficient AUV propulsors, thus extending the operational capabilities of these vehicles and providing stealth due to their low frequency operation.

Future work is directed towards further verification of the developed BEM solver via comparisons with the NTUA in-house developed MaPFlow RANS solver (Papadakis 2014) to determine whether effects of flow separation and dynamic stall affect the trends that the GPU-BEM solver reveals during this study. Finally, effects of free surface and waves are also worth investigating for AUVs operating at small to moderate submergence depths based on their mission. The study of more complex modal shapes for a wing with active deformation is an interesting topic of research that is also left for future work.

ACKNOWLEDGEMENTS

The present work is supported by the Seatech H2020 project and has received funding from the European Union's Horizon 2020 research and innovation program under the grant agreement No 857840. The opinions expressed in this document reflect only the author's view and in no way reflect the European Commission's opinions. The European Commission is not responsible for any use that may be made of the information it contains. Ms. D. Anevlavi is a recipient of the Special Account for Research Funding (E.L.K.E.) of National Technical University of Athens (N.T.U.A.) Scholarship Program for doctoral studies.

REFERENCES

Amoroso, C., A. Liverani, D. Francia, and A. Ceruti. 2021. "Dynamics augmentation for high speed flying yacht hulls through pid control of foiling." *Ocean Engineering* 108115.

Anevlavi, D., E. Filippas, A. Karperaki, and K. Belibassakis. 2022. "Optimization of a flexible flapping-foil thruster based on a coupled bem-fem model." *Volume 5B: Ocean Engineering; Honoring Symposium for Professor Gunther F. Clauss on Hydrodynamics and Ocean Engineering.* Hamburg: ASME. 1-10.

Anevlavi, D., E. Filippas, and K. Belibassakis. 2023. "Energy-minimizing kinematics for actively moprhing flapping-foil thrusters (under review)." *The 8th International Symposium on Ship Operations, Management & Economics (SOME).* 7-8 March, Athens, Greece: SNAME.

Barbarino, S., O. Bilgen, R. M. Ajaj, M. I. Friswell, and D. J. Inman. 2011. "A review of morphing aircraft." *Journal of Intelligent Material Systems and* 823–877.

Barrett, D. S. 1996. *Propulsive efficiency of a flexible hull underwater vehicle, Ph.D. thesis.* Massachusetts: Department of Ocean Engineering MIT.

Belibassakis, K., E. Filippas, and G. Papadakis. 2021. "Numerical and experimental investigation of the performance of dynamic wing for augmenting." *Journal of Marine Science and Engineering* 24.

Belibassakis, K., T. Gerostathis, K. Kostas, C. Politis, P. Kaklis, A. Ginnis, and C. Feurer. 2013. "A bem-isogeometric method for the ship wave-resistance problem." *Ocean Engineering* 53–67.

Fejtek, I., and J. Nehera. 1980. "Experimental study of flapping wing lift and propulsion." *Aeronautical Journal* 84: 28-33.

Filippas, E.S, and K.A Belibassakis. 2022. "A nonlinear time-domain bem for the performance of 3d flapping-wing thrusters in directional waves." *Ocean Engineering* 110157.

Filippas, E.S. 2019. *Hydrodynamic analysis of ship and marine biomimetic systems in waves using GPGPU programming, Ph.D. Thesis.* Athens: NTUA.

Filippas, E.S., and K.A. Belibassakis. 2014. "Hydrodynamic analysis of flapping-foil thrusters operating beneath the free surface and in waves." *Engineering Analysis with Boundary Elements* 47-59.

Filippas, E.S., G.P Papadakis, and K.A. Belibassakis. 2020. "Free-Surface Effects on the Performance of Flapping-Foil Thruster for Augmenting Ship Propulsion in Waves." *Journal of Marine Science and Engineering* 357.

Heathcote, S., Z. Wang, and I. Gursul. 2008. "Effect of spanwise flexibility on flapping wing propulsion." *Journal of Fluids and Structures* 183–199.

Lauder, G.V. 2000. "Function of the Caudal Fin During Locomotion in Fishes: Kinematics, Flow Visualization, and Evolutionary Patterns1." *American Zoologist* 40 (1): 101-122.

Li, D., S. Zhao, A. D. Ronch, J. Xiang, J. Drofelnik, Y. Li, L. Zhang, et al. 2018. "A review of modelling and analysis of morphing wings." *Progress in Aerospace Sciences* 46–62.

Li, Y., Z. Pan, and N. Zhang. 2011. "Propulsive properties of a flexible oscillating wing with time-varying camber deformation." *Ocean Engineering* 109332.

Liao, Yingqian, Joaquim R.R.A. Martins, and Yin Lu Young. 2021. "3-D high-fidelity hydrostructural optimization of cavitation-free composite lifting surfaces." *Composite Structures* 113937.

M. Ghommem, M. R. Hajj, D. T. Mook, B. K. Stanford, P. S. Beran, R. D. Snyder, L. T. Watson. 2012. "Global optimization of actively morphing." *Journal of Fluids and Structures* 210–228.

MATLAB. n.d. "n.d. Software Package, Ver. 2022a. Natick, MA: The MathWorks, Inc."

Mitsubishi. n.d. https://www.mhi.com/products/ship/finstabilizer.html.

Moran, J. 1984. *An Introduction to Theoretical and Computational Aerodynamics.* New York: John Wiley & Sons.

Neef, M. F., and D. Hummel. 2002. "Euler solutions for a Finite-Span Flapping Wing." *E. Krause et al. (eds.), High Performance Computing in Science and Engineering '01.* Berlin Heidelberg: Springer-Verlag. 386-395.

Neira, J., C. Sequeiros, R. Huamani, E. Machaca, and P. Fonseca: W. Nina. 2021. "Review on unmanned underwater robotics, structure designs, materials, sensors, actuators, and navigation control." *Journal of Robotics* 2021.

Ntouras, D., G. Papadakis, and K. Belibassakis. 2022. "Ship bow wings with application to trim and resistance control in calm water and in waves." *Journal of Science and Marine Engineering* 492.

Papadakis, G. 2014. *Development of a hybrid compressible vortex particle method and application to external problems including helicopter flows, Ph.D. Thesis.* Athens: NTUA.

Papadakis, G., E. Filippas, D. Ntouras, and K. Belibassakis. 2019. "Effects of viscosity and nonlinearity on 3d flapping-foil thruster for marine applications." *OCEANS 2019.* Marseille. 1-10.

Parolini, N., and A. Quarteroni. 2005. "Mathematical models and numerical simulations for the america's cup." *Comput. Methods Appl. Mech. Engrg* 1001–1026.

Prabahar, N. S. S., A. Persson, and L. Larsson. 2022. "Split-Flaps – a Way to Improve the Heel Stability of T-Foil Supported Craft." *Journal of Sailing* 1–30.

Salazar, R., V. Fuentes, and A. Abdelkefi. 2018. "Classification of biological and bioinspired aquatic systems: A review." *Ocean Engineering* 75–114.

Sfakiotakis, M., D. Lane, and J. Davies. 1999. "Review of fish swimming modes for aquatic locomotion." *IEEE Journal of Oceanic Engineering* 24 (2): 237–252.

Shi, Weichao, Roslynna Rosli, Mehmet Atlar, Rosemary Norman, and Dazheng Wang. 2016. "Hydrodynamic performance evaluation of a tidal turbine with leading-edge tubercles." *Ocean Engineering* 246-253.

Shyy, W., H. Aono, S. Chimakurthi, P. Trizila, C.-K. Kang, C. Cesnik, and H. Liu. 2014. "Recent progress in flapping wing aerodynamics and aeroelas-." *Engineering Analysis with Boundary Elements* 284–327.

SKF. n.d. https://www.skf.com/group/industries/marine/stabilizing-systems-and-steering-gear/retractable-fin-stabilizers-type-s.

Stanford, B. K., and P. S. Beran. 2010. "Analytical sensitivity analysis of an unsteady vortex-lattice method for flapping-wing optimization." *Journal of Aircraft* 647–662.

Thielicke, William, and Eize J. Stamhuis. 2018. "The effects of wing twist in slow-speed flapping flight of birds: trading brute force against efficiency." *Bioinspiration & Biomimetics: IOP Publishing* (IOP) 056015.

Triantafyllou, M. S., F. Hover, A. Techet, and D. Yue. 2005. "Review of hydrodynamic scaling laws in aquatic locomotion and fishlike swimming." *ASME. Appl. Mech. Rev.* 58: 226–237.

Vest, Michael S., and Joseph Katz. 1996. "Unsteady aerodynamic model of flapping wings." *AIAA* 1435-1440.

Wei, Zhaoyu, T.H. New, and Y.D. Cui. 2015. "An experimental study on flow sepration control of hydrofoils with leading-edge tubercles at low Reynolds number." *Ocean Engineering* 336-349.

Won-Shik, C., L. Kyung-Tae, S. Sung-Hyuk, H. Min-Woo, L. Jang-Yeob, K. Hyung-Soo, K. Min-Soo, P. Yong-Jai, C. Kyu-Jin, and A. Sung-Hoon. 2012. "Review of biomimetic underwater robots using smart actuators." *International Journal of Precision Engineering and Manufacturing* 13: 1281–1292.